FIVE-POINT BENDING TESTS ON 18MND5 CRUCIFORM SPECIMENS TO DEMONSTRATE THE WARM PRE STRESSING EFFECT

C.Jacquemoud[1], T.Yuritzinn[1], S.Marie[1], D.Moinereau[2], M.Nedelec[3], S.Chapuliot[4]
[1]CEA Saclay, DEN/DM2S/SEMT/LISN, Gif-sur-Yvette, FRANCE
[2]EDF, R&D division, MMC department, Moret-sur-Loing, FRANCE
[3]IRSN/DSR/SAMS, Fontenay-aux-Roses, FRANCE
[4]AREVA NP, Paris La Défense, FRANCE
E-mail of corresponding author: clementine.jacquemoud@cea.fr

ABSTRACT

In the framework of NESC VII European project, a large experimental program has been dedicated to demonstrate the Warm Pre Stressing (WPS) effect in different testing configurations. One of the CEA (France) contributions to this project is the realization of five-point bending tests on large cruciform specimens considering different WPS loading cycles. The five cruciform specimens, sponsored by EDF (France) and IRSN (France), are made of 18MND5 steel. The first two of them have been tested under a same LCF (Load-Cool-Fracture) loading cycle, including an isothermal preloading at T_{WPS} = -30°C followed by a cooling down to T_{FRAC} = -150°C at a constant load before an isothermal reloading up to fracture at T_{FRAC}. A more complex and realistic loading cycle have been considered for the following two specimens. They have been tested under a LCTF (Load-Cool-Transcient-Fracture) loading cycle, including an isothermal preloading at T_{WPS} = -30°C followed by a first cooling phase down to T_{unload} = -110°C at a constant load and a second cooling phase down to T_{FRAC} = -150°C with a decreasing load before an isothermal reloading up to fracture at T_{FRAC}. The results presented in this paper give a successful demonstration of the Warm Pre Stressing effect in biaxial loading conditions under both LCF and LCTF cycles.

INTRODUCTION

NESC VII is a European project concerning the relevance and the applicability of the Warm Pre Stressing effect in the Reactor Pressure Vessel (RPV) integrity assessment. The WPS effect represents the benefits of a warm preloading (in the ductile domain) on the effective toughness of the material at a lower temperature (in the brittle domain). It has been largely studied and might be considered in RPV integrity assessment during a Pressurized Thermal Shock (PTS). Considering the LCF (Load-Cool-Fracture) loading cycle as an example, represented in blue on Fig. 1, no cleavage fracture occurs during the cooling phase at a constant load since the material is warm preloaded. A reloading up to point B (Fig. 1-a) is necessary in order to observe cleavage fracture. Consequently, the main benefit of the warm pre stressing is the increase of the effective toughness comparing to the conventional isothermal toughness of the material (point C in Fig. 1-a). The new effective tenacity is directly dependant of the warm preloading level K_{JWPS} (point A in Fig. 1-a). The positive effect of the warm pre-stressing is similar on LCTF loading cycles (Fig. 1-b). Thus, this effect might help in a safety demonstration even if it will not constitute the basis of the demonstration yet.

The Work Package 1 (WP1) of NESC VII European project has been dedicated to experiments with the aim of demonstrating the WPS effect in loading conditions representative of PTS conditions. In addition to standard specimen testing, the project partners intend to demonstrate the WPS effect in biaxial loading conditions using cruciform specimens. Five cruciform specimens were considered in NESC VII project: they were made of 18MND5 ferritic steel and sponsored by EDF (France) and IRSN (France). The CEA (France) contribution to WP1 is the realization of five-point bending tests on these large cruciform specimens considering different WPS loading cycles. The first two specimens have been tested on the same LCF loading cycle, including an isothermal preloading at T_{WPS} = -30°C followed by a cooling down to T_{FRAC} = -150°C at a constant load before an isothermal reloading up to fracture at T_{FRAC}. A more complex and realistic loading cycle have been considered for the following two specimens. They have been tested under a LCTF (Load-Cool-Transcient-Fracture) loading cycle, including an isothermal preloading at T_{WPS} = -30°C followed by a first cooling phase down to T_{unload} = -110°C at a constant load and a second cooling phase down to T_{FRAC} = -150°C with a decreasing load before an isothermal reloading up to fracture at T_{FRAC}. The first goal is to demonstrate that biaxial loading conditions do not question the WPS effect either on a simple LCF loading cycle or on a LCTF loading cycle. The second one is to verify the reproducibility of this type of test. To make the demonstration relevant, the loading level K_{JWPS} during the cooling phase has to be high enough so that the toughness curve is crossed during the cooling phase of a LCF cycle but not too high to avoid non expected effects as extended plasticity. The selected K_{JWPS} level for LCF cycles is about 80 MPa.m$^{0.5}$ corresponding to the mean K_J value along the crack tip. This value is consistent with the maximal loading conditions undergone by a French PWR vessel during a PTS. The same K_{JWPS} level is used for LCTF loading cycle; the K_J level at the end of the unloading phase is chosen close to 45 MPa.m$^{0.5}$ to be below the toughness curve at T_{FRAC} = -150°C .

This paper focuses on the first four tests performed on cruciform specimens either under LCF or LCTF loading cycles; the testing procedure and the experimental results concerning the four tests are presented below. The last section concentrates on the interpretations of the LCF tests mainly.

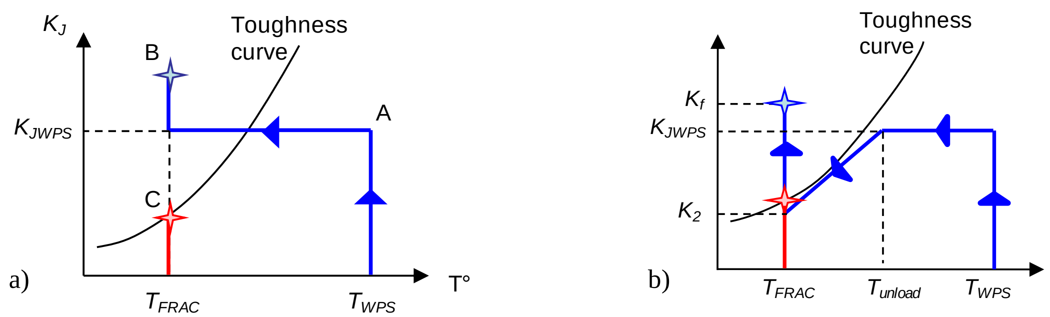

Fig.1: WPS effect on a LCF loading cycle (a) and LCTF loading cycle (b)

EVALUATION OF THE BIAXIAL EFFECT ON THE APPARENT TOUGHNESS OF CRUCIFORM SPECIMENS

Model description

A 3D mesh of one quarter of the cruciform specimen is generated with CASTEM® [1] using quadratic parallelepiped and prismatic elements (Fig. 2-b). The crack tip is represented by one quarter of an ellipse. Each specimen is meshed independently with its exact crack dimensions measured experimentally on the fractured surface, in order to simulate each of the two tests with its proper conditions (load, temperature, crack dimensions). The finite element analyses have been performed using an elastic plastic isotropic constitutive law that was a function of the temperature.

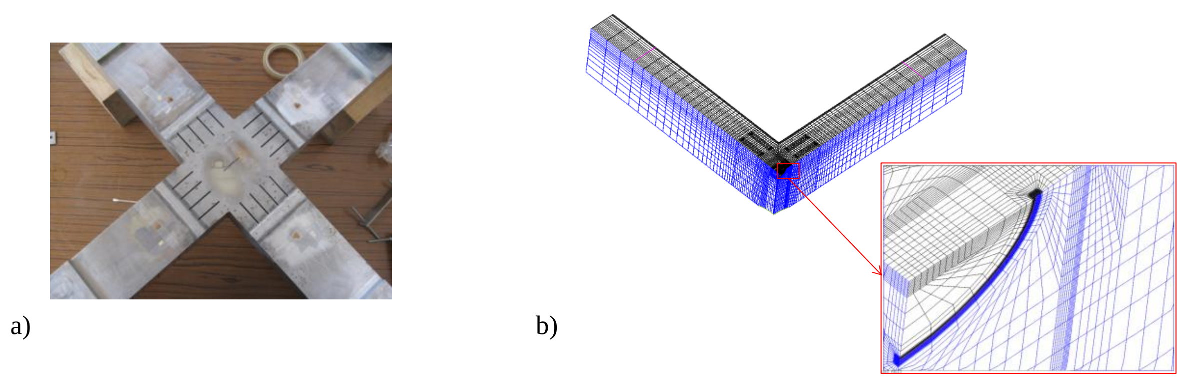

Fig.2: The cruciform specimen and its 3D mesh

Considering a global approach, the non-linear strain energy release rate J is calculated from small displacements and strains finite element analysis using a post-treatment procedure implemented in CASTEM®. The elastic plastic stress intensity factor K_J is deduced from Eq. 1:

$$K_J = \sqrt{\frac{E.J}{1-\nu^2}} \tag{1}$$

where E is the Young modulus and ν the Poisson coefficient of the material. A mean $K_{J\text{mean}}$ value along the elliptical crack tip is determined using a simplified version of the expression proposed by Wallin [2]:

$$K_{J\,mean} = \left(\int_0^L K_J(l)^4 . \frac{dl}{L} \right)^{1/4} \tag{2}$$

where L is the crack tip length.

Beremin local approach is also considered for fracture probability calculation. Even though it is not the best model for geometry-related effect modeling, it is a good fracture indicator. The Beremin initial formulation [3] takes into account the two phases of the brittle fracture process: nucleation, when a micro-crack forms, followed by propagation, when the macro-crack becomes unstable and causes instability of the surrounding matrix. The model does not quantify the nucleation phase but deals with it implicitly by assuming that the nucleation criterion is constantly met in the zone where plasticity is active. In other words, there is always an available micro-defect in every elementary volume where plasticity is developing that can lead to failure. The fracture criterion is then based on the maximal principal stress, used with a Weibull model to establish a fracture probability for a given level of principal stress. In this approach, the loaded volume (the volume susceptible to contain cracks, i.e. the plastic volume) is divided into n elementary volumes v_0 in which prevails a stress state described by the maximal principal stress σ_1. If the weakest link hypothesis is adopted, the following can be written:

$$P_R = 1 - exp\left\{ -\left(\frac{\sigma_W}{\sigma_u} \right)^m \right\} \text{ with } \sigma_W = \left[\int_{V_p} \left[\sigma_1 . exp\left(-\frac{\varepsilon_p}{2} \right) \right]^m . \frac{dv}{v_0} \right]^{\frac{1}{m}} \tag{3}$$

It can be noticed that the present formulation allows for plastic strain so as to represent the reduction in the harmfulness of micro-cracks by blunting and transverse contraction. It represents a Weibull distribution (expressed with no threshold), where σ_W is the Weibull stress, m the Weibull modulus and σ_u the cleavage stress. In addition, in this equation, v_0 must be defined around the size of a few grains, small enough for the stress gradient in v_0 to be disregarded and large enough to be able to determine the possibility of finding a crack. $(50\mu m)^3$ was chosen in our application. To account for load history effects, a modified formulation [4] was proposed including supplementary assumptions: initiation of cleavage at the damage site can only occur when plasticity is active, i.e. when strain-hardening variable $\dot{p}$ is positive. The model depends on the maximum stress history and the temperature history at all points in the structure studied. This relationship with temperature has made it possible to consider dependency of the critical cleavage stress on temperature. The combined probability of fracture of the structure at an instant t is thus now written as follows:

$$P_R(t) = 1 - exp\left[-\int_{V_p} \left[\max_{(\tau \le t, \dot{p}(\tau) > 0)} \frac{\sigma_1(\tau)}{\sigma_u(T(\tau))} exp\left(-\frac{\varepsilon_p(\tau)}{2} \right) \right]^m \frac{dv}{v_0} \right] \tag{4}$$

where $\sigma_1(\tau)$ is the maximal principal stress at instant τ, $\sigma_u[T(\tau)]$ is the characteristic cleavage stress which depends on the temperature $T(\tau)$. The Weibull stress at instant t is now defined by convention at a reference temperature T_{ref} to obtain an expression equivalent to the initial Beremin formulation (3):

$$\sigma_W(t) = \sigma_u(T_{ref}) . \left[\int_{V_p} \left[\max_{(\tau \le t, \dot{p}(\tau) > 0)} \frac{\sigma_1(\tau)}{\sigma_u(T(\tau))} exp\left(-\frac{\varepsilon_p(\tau)}{2} \right) \right]^m \frac{dv}{v_0} \right]^{\frac{1}{m}} \tag{5}$$

Large displacements and strains finite element analysis is dedicated to the fracture probability P_R calculation using the modified Beremin model.

Numerical results

As an isothermal toughness representative of biaxial loading was not measured through tests, it is evaluated from finite element simulations of an isothermal loading at a temperature of -150°C corresponding to the fracture temperature of the WPS cycles analyzed in this study. Considering Beremin model, the aim is to compare the fracture probability distribution of the cruciform specimen, which is considered to have a small defect, to the experimental and simulated results obtain on Compact Tensile (CT) specimens with a large defect (a/t = 0.5) and Single Edge Notched Specimens (SENB) with a small defect (a/t = 0.1). Figure 3 presents the experimental fracture toughness distribution for the CT and SENB specimens made of the same 18MND5 material as the cruciform specimen and tested at -150°C by the CEA (France). In addition, the Beremin model is applied to the CT, the SENB and the cruciform specimen numerical results so the corresponding fracture probability distribution is plotted on Fig. 3 for each of the three specimen types.

Comparing experimental toughness distributions, an important geometry-related effect is observed on the distribution of the K_J values at fracture but no geometry-related effect appears for the lower K_J values. The distribution of the fracture probability evaluated with Beremin model for the cruciform specimen is closer to the experimental toughness distribution of the CT specimens (with a/W = 0.5) than the SENB specimens (with a/W = 0.1). This indicates that the short crack effect is reduced for large crack dimensions as those of the cruciform specimen. Consequently, the loading conditions for the cruciform specimen are defined using the master curves corresponding to the CT specimens as a reference. The K_{JWPS} level of 80 MPa.m$^{0.5}$ is chosen close to the 95% master curve at -150°C.

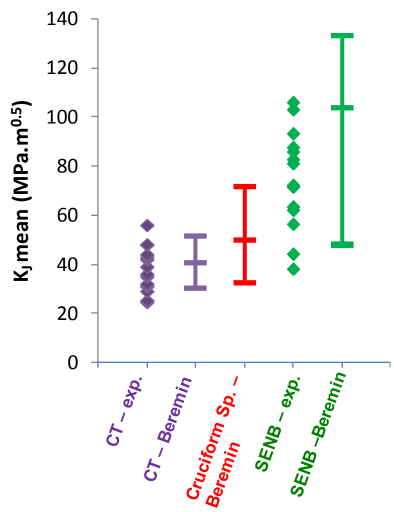

Fig.3: Experimental fracture toughness of CT and SENB specimens and Beremin predictions (P_R = 5%-50%-95%) for CT, SENB and cruciform specimens for isothermal loadings at -150°C

BENDING TESTS

Testing procedure

All cruciform specimens (specimen 1 to 4) presented in this paper are made of 18MND5 steel and have similar dimensions (Fig. 2-a). A semi-elliptical notch has been initially machined in each specimen and then extended by fatigue pre-cracking so that the ratio a/W (a = crack depth, W = thickness) is equal to 0.12 for specimen 1, to 0.13 for specimen 2, to 0.125 for specimens 3 and 4. A five-point bending device has been especially designed by the CEA to be adapted to a 2500-kN tensile test machine. The bending device is placed inside a large thermal chamber cooled with nitrogen.

The CMOD is measured with a clip gage (MTS 632-03F-31, n°1266515, operating temperature: -270°C/+65°C) and the specimen deflection is obtained from a deflection measurement device specifically designed and adapted to the cruciform bending tests. The CMOD value and the deflection value recorded experimentally do not correspond to the real ones during the cooling phase of the WPS cycle. Both measurement devices (clip gage and deflection measurement device) have to be temperature calibrated before the test, in order to determine the correction equation governing each device retraction with the temperature. This correction is then applied to the experimental value recorded during the test. In addition, each specimen is equipped with three type K thermocouples (Fig; 4-a) from which the specimen mean temperature is calculated. A preliminary test on a cruciform specimen equipped with through thickness thermocouples demonstrated that the temperature was homogeneous inside the specimen with the present cooling procedure and that the temperature measured by the thermocouples on the surface was representative of the specimen temperature. The clip gage and the deflection measurement device are also equipped with type K thermocouples in order to measure precisely the device temperature to be used in the correction equation. Finally, eight low temperature strain gages (Vishay WK-06-125AD-350) are placed on the specimen and four strain gages (CEA-09-125UW-120) are placed on the supporting columns of the bending device (Fig; 4-b) in order to verify, before each test, the balance of the entire testing device and the symmetry of the loading.

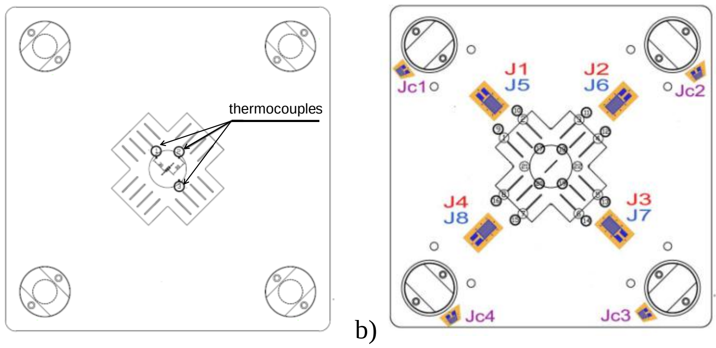

a) b)

Fig.4: Thermocouple (a) and strain gage (b) positions on the cruciform specimen

Prior to each test, a fatigue pre-cracking has been performed on the 2500-kN tensile test machine, under a cyclic compressive loading at a constant temperature of 10°C. The fatigue pre-cracking is divided into four steps with decreasing loading level so that the initial ΔK value is about 25 MPa.m$^{0.5}$ and the final one is around 12 MPa.m$^{0.5}$.

The WPS loading cycle considered for the first two specimens (tests 1 and 2) is a LCF cycle including: a preloading phase up to a K_{JWPS} value of 80 MPa.m$^{0.5}$ at a constant temperature of T_{WPS} = -30°C, followed by a cooling down to T_{FRAC} = -150°C at a constant load, before an isothermal reloading up to fracture at T_{FRAC}. The following two specimens (tests 3 and 4) have been tested under a LCTF cycle including: an isothermal preloading up to a K_{JWPS} value of 80 MPa.m$^{0.5}$ at a constant temperature of T_{WPS} = -30°C, followed by a first cooling phase down to T_{unload} = -110°C at a constant load and a second cooling phase down to T_{FRAC} = -150°C with a load decreasing to a K_{unload} value of 45 MPa.m$^{0.5}$, before an isothermal reloading up to fracture at T_{FRAC}.

After the tests, the fractured specimens have been scanned and the exact dimensions of the crack have been measured for each specimen.

Experimental results

For all tests, the final cleavage fracture has occurred during the last isothermal reloading phase at T_{FRAC} = -150°C, so the ultimate load is clearly higher than the maximal loading level reached during the warm pre loading phase, whatever the WPS cycle type is. Moreover, Fig. 5 shows that the fractured specimen shapes are similar.

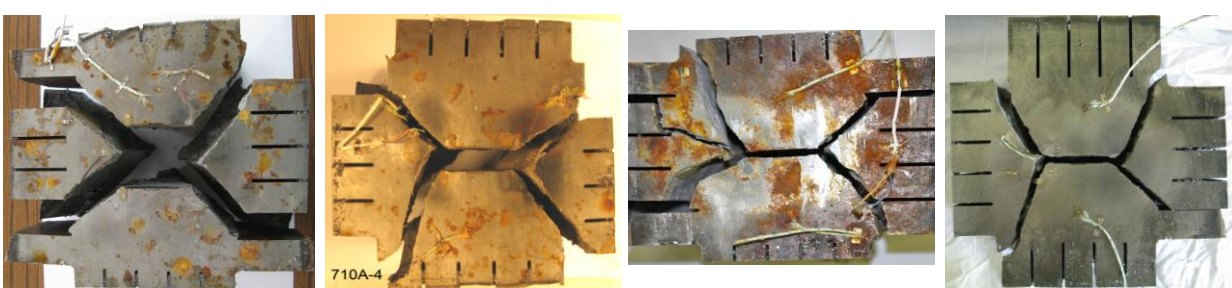

a) b) c) d)

Fig.5: Fractured specimens of LCF tests 1 (a) and 2 (b) and LCTF tests 3 (c) and 4 (d)

BENDING TEST INTERPRETATIONS

This section presents the interpretations of the two LCF tests realized by finite element analysis considering the global approach and the Beremin model. An engineering approach proposed by EDF-AREVA-CEA is also presented. In further works, Wallin [2] and Chell&Haigh [5] models will also be considered for test interpretations and compared to the present study.

Global approach

Figure 6-a represents the evolution of the mean value of K_J with the temperature during the LCF loading cycle. Both specimens undergo similar loading paths. Consequently their fracture characteristics are very close. Indeed, the simulated K_J mean value, corresponding to the experimental ultimate load, is given in Tab. 1 for test 1 and test 2. No main difference is noticed between the two values excepting the slight influence of a larger crack for specimen 2. The ultimate K_J values are both higher than the K_{JWPS} value of 80 MPa.m$^{0.5}$.

Table 1: Simulated K_J mean value and Beremin fracture probability corresponding to the experimental ultimate load for tests 1 and 2

	Test 1	Test 2
K_J mean (MPa.m$^{0.5}$)	96.7	98.4
P_R (%)	95	96.5

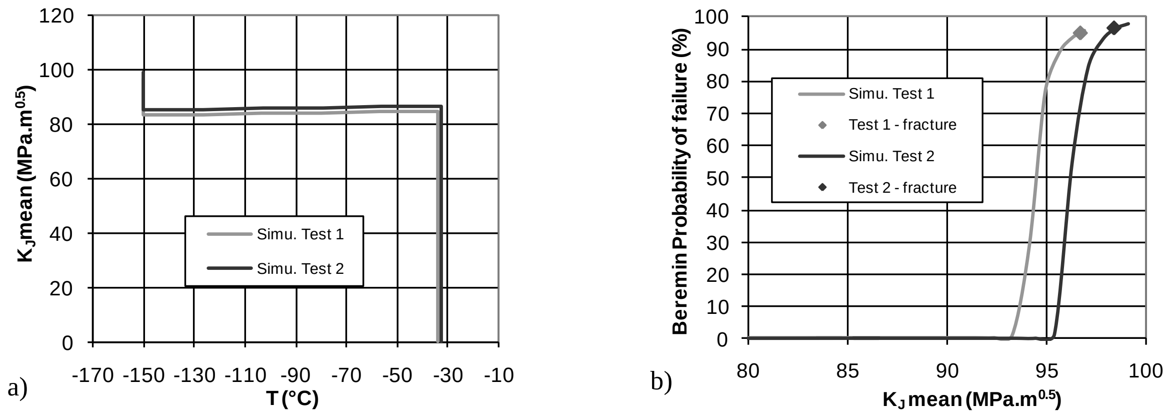

Fig.6: Simulated K_J mean value versus temperature for test 1 and test 2 (a) and simulated Beremin fracture probability versus K_J mean value for tests 1 and 2 (b)

The modified Beremin model

According to the Beremin model, the fracture probability corresponding to the experimental fracture load is given in Tab. 1 for test 1 and test 2 and also plotted in Fig. 6-b on the fracture probability evolution with the K_J mean value. At the time of the experimental fracture, the fracture probability is higher than 95% for both tests.

Engineering approach

In order to reach the final goal of WPS principle codification in the RSE-M standard, a large R&D program has been going on within French or European programs for few years, in order to provide all the necessary arguments for a criterion proposition and validation. The very large amount of experimental and numerical results gained up to now allows us to propose today a criterion for fracture evaluation under thermo-mechanical loading.

Studies on WPS benefit illustration started in the early 1980's in the UK with the significant work of Chell [6] and Curry [7] and have been carried on up to now all over Europe in order to illustrate, quantify, develop or validate criteria. The first step in the criterion proposition has been to take advantage of all these past works in order to constitute an extensive and convincing database of experimental results, including a variety of ferritic steels leading to different modes of fracture, of specimen geometries and sizes, of thermo-mechanical transients and complementary mock-up tests with various loading types and defect shapes. The experimental data included in the database today are the following:

- 18MND5 French material in as received state (data coming from the SMILE European project [8], from additional publications [9,10] and completed by the preliminary mock-up test and the 2 LCF tests presented in this paper, all performed within the NESC VII project);
- WPS1, WPS2 and WPS3, German steels in as received and thermally aged states (data obtained by MPA Stuttgart [11] and completed by the mock-up test performed in the SMILE project [8]);
- EN3 low alloy steel undergoing cleavage fracture [12];
- EN36 cast Ni-Cr steel in tempered or thermally degraded states, undergoing cleavage, mix cleavage-intergranular of fully intergranular fracture [12];
- A533 in thermally aged state undergoing intergranular fracture [12];
- Recent NRI tests performed on WWER 440 RPV steel, in as received and irradiated states [13,14].

Within this database (containing approximately 460 tests), a large number of different configurations can be investigated. This allows an extensive validation of the criteria based on the evaluation of different effects, mainly due to the material behaviour, the material state, the potential material degradations, the fracture mode, the size and loading form (tensile, bending and thermal loading, small to very large specimen) or the Temperature-Load history (transient shapes). This database has been used with the objective to validate as much as possible the criterion transferability from laboratory specimens to a real PTS case [15].

The loading parameter definition for the criterion has been directly based on all these experimental results. As the maximal loading level at the warm temperature (K_{JWPS}) appeared to be a key parameter of the problem, it has been decided to propose a criterion referring to this maximal loading level and to check, for different transient shapes, the distance from K at fracture (noted K_f) to the maximal loading level. Thus, two parameters have been introduced (see Fig. 1-b for K_J level definitions) and are defined in Eq. (6): the relative unloading during the transient, characterised by the parameter U_{nl} and the reloading capability, characterised by the parameter R_{cap}.

$$U_{nl} = \frac{K_{JWPS} - K_2}{K_{JWPS}} \text{ and } R_{cap} = \frac{K_f - K_2}{K_{JWPS}} \tag{6}$$

According to this definition, classical WPS transients can be classified as follows:

- LCF cycles correspond to $U_{nl} = 0$ (no unloading, $K_2 = K_{JWPS}$);
- LUCF & LTUF cycles correspond to $U_{nl} = 1$ ($K_2 = 0$, maximum unloading);
  LPTUF & LPUCF cycles correspond to intermediate unloading values ($U_{nl} \sim 0.5$).

a) 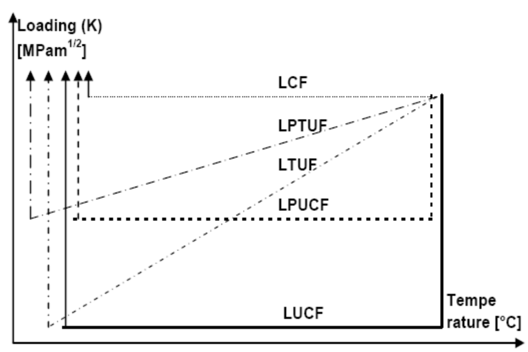

b) 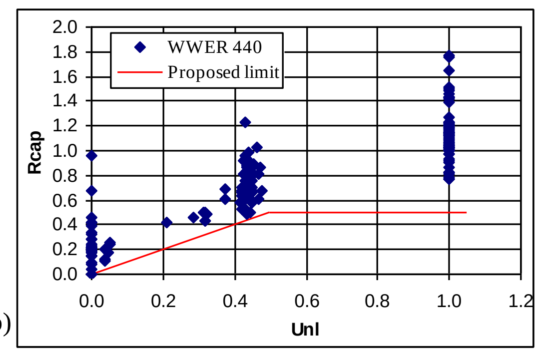

Fig.7: Loading transient shapes definition in NRI tests (a) and NRI tests results in the U_{nl}-R_{cap} space (b)

Following the database constitution and the loading parameters definition, the third step has been the criterion formulation based on the interpretation of the largest series of tests; i.e. the recent NRI test results. They represent a huge number of tests (Pre-cracked Charpy Notched specimens – 3-point bending tests with a/W close to 0.5) performed under different loading transients (Fig. 7-a) and corresponding to unloading parameters U_{nl} varying from 0 to 1. The K_{JWPS}, K_2 and K_f values used for this interpretation are those determined by the complementary F.E. analysis presented in [14]. Figure 7-b gives a representation of NRI test results in a U_{nl}-R_{cap} space. It clearly appears that the following limit curve (red line on Fig. 7-b) is an envelope for all the experimental data:

- For limited partial unloading ($U_{nl} < 0.5$), no effect on the reloading capability is observed. The unloading stress field at the crack tip remains quasi-elastic and thus the material is not affected. A supplementary loading ($R_{cap} > U_{nl}$) is needed, so that a reasonable envelope can be defined by: $R_{cap} = U_{nl}$
- For larger partial unloading ($U_{nl} < 1$), stress unloading is larger and plasticity in compression may occur at the crack tip. Material/residual stresses/crack tip blunting are affected and reloading capability may become lower than unloading ($R_{cap} < U_{nl}$). A reasonable envelope, $R_{cap} = 0.5$, is chosen to define the reloading limit.

The criterion formulation is then:

$$K_{chap} = max(K_{IC}(T);min(K_{wps};K_2 + K_{WPS}/2)) \tag{7}$$

All the other non irradiated tests available in the database are then interpreted and represented in the same U_{nl}-R_{cap} space on Fig. 8. On Fig. 8-a presenting Cheng & Noble results (3-point bending tests), T refers to tests presenting a trans-granular mode of fracture, I and inter-granular mode of fracture and 50%T a mix between the 2. Figure 8-b concerns 18MND5 tests (1TCT tests under LCF and LUCF loading paths), MPA tests (WPS1, WPS2 and WPS3 tests performed on 1T to 4T CT specimen), CT_{por} tests (on CT specimen containing semi-elliptical cracks [10]) and structural tests (performed on mock-ups). The details concerning the mock-up tests available in the database are given on Fig. 8-b. In this category, different thermo-mechanical loadings have been investigated: tensile tests with large or small cracks, uniaxial and biaxial loading, thermal shocks or tests with mock-up at constant temperature. The results of the two LCF tests performed on cruciform specimens and presented in this paper are also included. The values of R_{cap} calculated for two LCF tests are both equal to 0.14. The proposed limit appears to be a reasonable envelope for all available results in the experimental database. Only one test is below the limit. It was identified in [15] that this test was the one with the highest imposed K_{JWPS} (167 MPa.m$^{0.5}$), which is not representative of the levels encountered in the RPV. The mock-up tests are merged in the dispersion of the CT specimen tests: geometry-related or loading type effects have a limited influence on the fracture behavior during reloading. At this step, the proposed limit is considered as a good candidate for fracture definition.

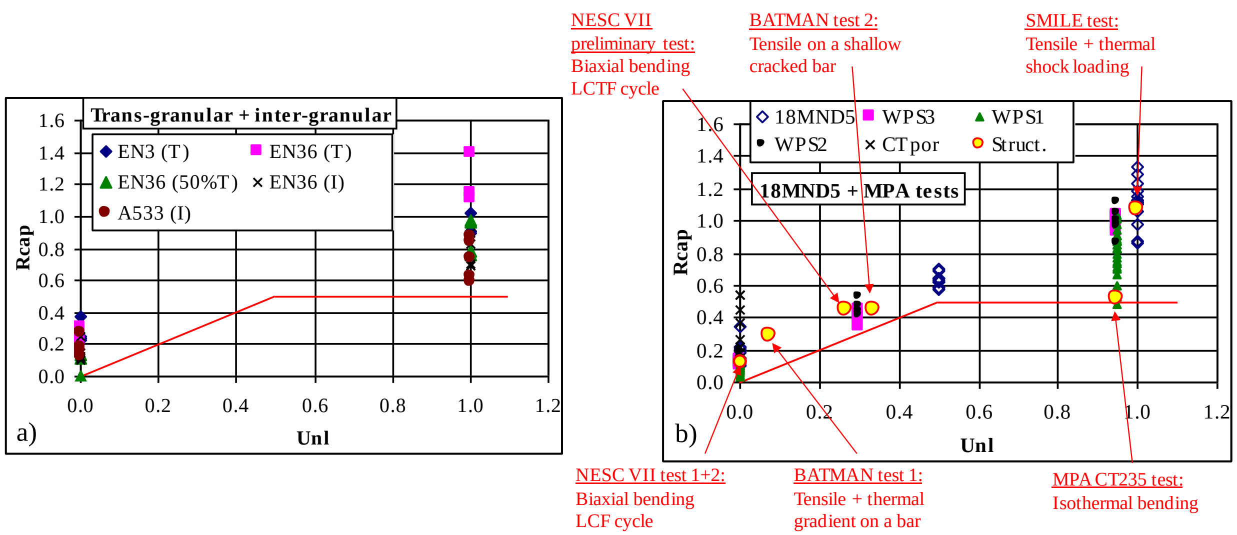

Fig.8: Cheng & Noble results interpretation (a) and 18MND5 + MPA WPS test interpretations with the details concerning the mock-up tests (b)

CONCLUSION

In the framework of NESC VII European project, the CEA (France) has designed and realized five-point bending tests on 18MND5 cruciform specimens with the objective to demonstrate the warm pre-stressing effect in biaxial loading conditions. A LCF loading cycle is considered for the first two bending tests. This cycle includes a preloading phase up to a KJ_{WPS} value of 80 MPa.m$^{0.5}$ at a constant temperature of T_{WPS} = -30°C followed by a cooling down to T_{FRAC} = -150°C at a constant load before an isothermal reloading up to fracture at T_{FRAC}. This paper focuses on these two tests; the experimental results are presented and completed by the interpretation of each test using finite element analysis.

Firstly, the final cleavage fracture has occurred during the last isothermal loading phase of all tests, so the ultimate loading level is clearly higher than the K_{JWPS} value of 80 MPa.m$^{0.5}$ reached during the warm preloading phase. These experimental results represent a successful demonstration of the WPS effect in biaxial loading conditions, when either a simple LCF cycle or a more realistic LCTF cycle are concerned. It is important to note that even though the preloading level (K_{JWPS} of 80 MPa.m$^{1/2}$) has been intentionally chosen close to the master curves of the material at the fracture temperature, the WPS benefits are visible. Secondly, considering each type of loading cycle, the ultimate K_J mean values as well as the fracture specimen shapes are similar. These results attest of the good reproducibility of these tests. The fifth cruciform specimen is to be tested under a loading history idealizing the loading undergone by a crack during a pressurized thermal shock in a pressurized water reactor.

First test interpretations on LCF loading cycles show that the results presented are in accordance with the simple criterion proposed for pre-codification [15]. The modified Beremin model gives fracture probabilities higher than 95% for LCF loading cycles, which also show the conservatism of the model in estimating WPS benefit. Once the five cruciform specimens are tested considering different types of WPS loading paths, we intend to compare Bermin local model to engineering approaches such as Wallin [2], Chell&Haigh [5] and the criterion presented in this paper.

REFERENCES

[1] CAST3M, http://www-cast3m.cea.fr/cast3m

[2] Wallin K., "Master curve implementation of the warm pre-stress effect", *Engineering Fracture Mechanics*, 70, 2003, pp. 2587–2602.

[3] Beremin F.M., "A local criterion for cleavage fracture of a nuclear pressure vessel steel", *Metallurgical Transaction A*, 14A, 1983, pp 2277-2287.

[4] Lefevre W. et al., "A modified Beremin model to simulate the warm pre-stress effect", *Nuclear Engineering and design*, Vol.216, 2002, pp 27-42.

[5] Chell G.G., "The effect of warm pre-stressing on proof tested pressure vessels", *Int. J. Pres. Ves. Piping*, Vol.23, 1980, pp 121-132.

[6] Chell G.G., and Haigh J.R., "Some fracture applications of warm pre-stressing to pressure vessels*", 4th int. Conf. on Press. Ves. Tech*., London, paper C22/80, 1986.

[7] Curry D.A., "A micromechanistic approach to the warm pre-stressing of ferritic steels", *Int. J. of fracture*, Vol.17(3), 1981.

[8] Moinereau D., et al., "SMILE project: the effect of WPS in RPV assessment. Synthesis of experimental results and analyses", *PVP2006-ICPVT11-93178*, 2006.

[9] Yuritzinn T., et al., "Illustration of the WPS benefit through BATMAN test series: Tests on large specimens under WPS loading configurations", *Engineering Fracture Mechanics*, Vol.75, 2008, pp. 2191-2207.

[10] Yuritzinn T., et al., "Warm pre-stressing tests on specimens with semi-elliptical cracks and analysis of the results", *Engineering Fracture Mechanics*, Vol.77, 2010, pp. 71-83.

[11] Alsmann U., 2002, "Untersuchungen zu den Mechanismen des Vorbelastungseffekts", *PhD thesis, Stuttgart University*, Stuttgart, Germany.

[12] Chen J., and Noble F.W.., "The Warm Pre Stressing in steels undergoing inter-granular fracture", *Fatigue Fract. Engng Mater. Struct*., Vol.20, 1997, pp. 1399-1411.

[13] Lauerova D., et al., "Warm Pre Stressing tests on WWER 440 reactor pressure vessel material*", PVP2009-77287*, 2009.

[14] Chapuliot S., et al., "Information about WPS experiments performed in NRI Rez and their evaluation", *Fontevrault 7*, Avignon, France, paper A083, 2010.

[15] Chapuliot S., et al., "WPS criterion proposition based on experimental data-base interpretation" *Fontevrault 7*, Avignon, France paper A141, 2010.